Journal of Environmental Chemical Engineering 14 (2026) 122822

Contents lists available at ScienceDirect

Journal of Environmental Chemical Engineering

journal homepage: www.elsevier.com/locate/jece

CO_2 storage as clathrate hydrates in natural marine sands: Formation behaviour and microstructural insights from Raman and SEM analyses

Beatrice Castellani [a,*], Sowjanya Kandadai [a], Umberta Tinivella [b], Michela Giustiniani [b], Lorenzo Remia [c], Rita Giovannetti [c], Marco Zannotti [c]

[a] Department of Engineering, University of Perugia, Via G. Duranti, Perugia, Italy
[b] Istituto Nazionale di Oceanografia e di Geofisica Sperimentale – OGS, Borgo Grotta Gigante 42C, Sgonico, TS 34010, Italy
[c] School of Science and Technology, ChIP Research Center, Chemistry Division, University of Camerino, Camerino 62032, Italy

ARTICLE INFO

Keywords:
CO_2 hydrates
CO_2 storage
Marine sediment
Geological storage
Offshore CCS
Clathrate hydrates

ABSTRACT

The storage of carbon dioxide (CO_2) in the form of clathrate hydrates in marine environments represents a promising strategy for mitigating climate change. Clathrate hydrates are crystalline structures formed when CO_2 molecules are trapped within water cages under conditions of low temperature and high pressure, commonly found in marine environments. This study investigates the storage performance, dissociation kinetics and microstructural characteristics of CO_2 hydrates formed in natural sand from the Adriatic Sea using a 1 L isochoric reactor. Hydrate formation in sand was compared to pure water systems to isolate the role of the natural sand. Results show that sand significantly enhances storage performance, increasing gas uptake (from 7.7% to 18.2% up to 9.7–36.7%) and water conversion rate (from 1.3% to 2.8% up to 4.0–8.5%), particularly at lower pressures. Temperature remains the dominant operating parameter, while heterogeneous nucleation and improved heat dissipation given by the sand promote hydrate formation. Raman and SEM analyses reveal that natural sand decreases molecular disorder and lead to denser hydrate morphologies, supporting enhanced conversion efficiency. These findings demonstrate that the studied natural sand acts as kinetic and interfacial promoter of hydrate-based CO_2 storage, providing quantitative insights relevant for offshore CCS strategies.

1. Introduction

Carbon capture and storage (CCS) technologies can play a crucial role in achieving the target of carbon dioxide (CO_2) emission reduction. According to the Clean Technology Scenario (CTS) developed by the International Energy Agency IEA, CCS development is expected to reach 115 CO_2 gigatonnes (Gt) involved by 2060, with 93% permanently stored [1]. To achieve this level of deployment will require a significant scale-up starting from current levels. CO_2 storage is a strategic component of the CCS actions and can be achieved through different pathways, which include also oceanic storage [2]. The most studied techniques are saline aquifers, depleted oil and gas reservoirs, unmineable coal seams, basalt formations. The majority of the global storage capacity (55000 Gt) is found onshore, primarily within deep saline formations and depleted oil and gas fields. There is also an offshore storage potential, estimated between 2000 and 13000 Gt [3]. In addition to the above mentioned options, there is also a novel pathway for CO_2 storage, which is based on gas hydrates. To obtain hydrate-based storage, it is necessary to comprehend the properties governing CO_2 hydrate formation and dissociation.

Gas hydrates are nonstoichiometric crystalline compounds, which form under high pressures and low temperature when gas molecules encounter water. In such conditions, water naturally form hydrogen-bonded cages that encapsulate gas molecules via van der Waals forces, allowing for CO_2 entrapment within the crystalline structure [4]. This ability has gained significant attention, in the last years, for CO_2 capture and storage applications, since it is considered more efficient from energy and environmental points of view compared to traditional approaches [5,6], considering that 1 m^3 of hydrate can store 160–180 m^3 of CO_2 in standard conditions [4].

The widespread presence and long-term stability of natural gas hydrates, which have shown to be secure methane reservoirs for millennia, within sediments such as seafloors and permafrost zones, indicate significant potential for their use also in direct CO_2 storage. This application is particularly relevant in marine environments, where pressure and temperature conditions are naturally suitable for hydrate formation.

* Corresponding author.
E-mail address: beatrice.castellani@unipg.it (B. Castellani).

https://doi.org/10.1016/j.jece.2026.122822
Received 4 February 2026; Received in revised form 7 April 2026; Accepted 22 April 2026
Available online 24 April 2026

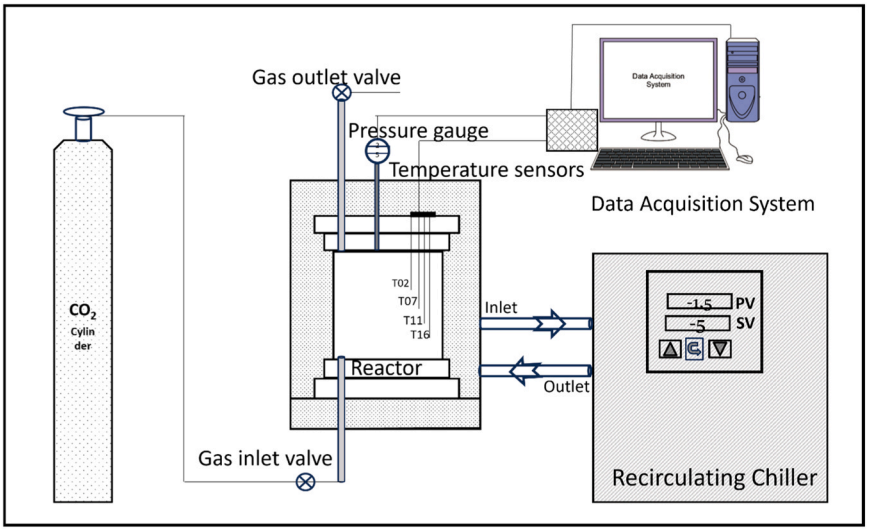

Fig. 1. Schematic diagram of the experimental setup.

In addition, the risk of potential leakage is reduced since, even in case of CO_2 hydrate dissociation, CO_2 can be entrapped again in the ascent pathway, forming hydrate caps and effectively preventing further escape [7].

As remarked also by IEA, technical factors related to geology are crucial for the development of CO_2 storage technologies. This is particularly important for CO_2 hydrates: it was shown in fact that the efficiency of CO_2 storage processes is highly sensitive to the complex interactions between water, sediment and the gas involved, affecting hydrate formation and storage capability [8].

The current understanding of the phenomena involved in gas hydrate formation and the physical properties of hydrate-bearing sediments in the natural environment is still limited, as described in the review paper of [9].

The main role of porous media in hydrate formation is giving heterogeneous nucleation sites [10]. Variations in the pore diameter and in the particle size significantly impact hydrate nucleation and growth mechanisms within porous media. Heeschen et al., [11] suggested that there is a significant particle size effect on the kinetics of gas hydrate formation, with fine grains making gas hydrate formation faster if compared to medium or coarse sands. This can be due to the enlarged mineral surface but also on the effect of specific minerals, like iron-oxy-hydroxide, which promote gas hydrate formation. Another effect of porous media is about heat transfer process, since they enhance nucleation by facilitating efficient heat dissipation during hydrate formation [12]. While research has demonstrated that natural sediments influence hydrate kinetics [13], there still remain large knowledge gaps regarding their behaviour in marine environments, considering that in nature there is a wide variability in sediment composition and morphology, as well as the presence of naturally occurring promoters such as dissolved ions and organic compounds [14].

In this context, isolating the intrinsic physical effect of the sediment itself represents a necessary step to disentangle the role of porous media from additional chemical contributions.

This study addresses these gaps by comparing CO_2 hydrate formation in pure water and with natural sand from the Adriatic Sea. This sediment is representative of permeable sandy layers commonly found in continental shelf and upper slope environments. While it does not encompass the full variability of marine sediments, it represents a relevant and well-defined subclass of geological formations. Hydrate formation in natural sand was investigated under different pressures and temperatures using a 1 L isochoric reactor designed to reproduce in-situ environments and assess the influence of natural sediments. A comparative analysis was performed to evaluate hydrate formation with and without sand, using

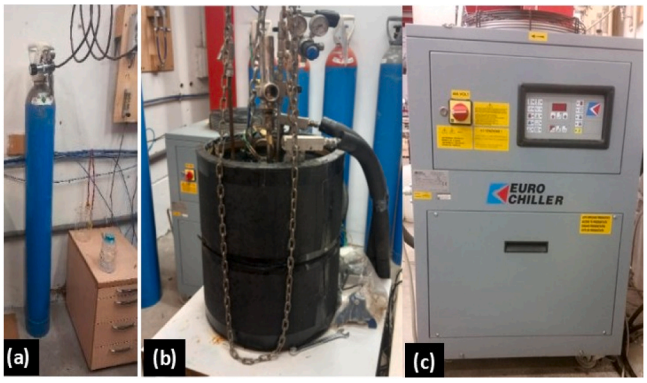

Fig. 2. (a) Gas cylinder (b) Reactor setup inside a thermostatic bath (c) Recirculating chiller.

performance indicators such as formation density and water-to-hydrate conversion. Complementary, SEM and Raman analyses were conducted on water, sand and CO_2 hydrate samples to correlate microscopic features with macroscopic behaviour. This integrated approach provides new insights into how natural sediments govern CO_2 hydrate formation and dissociation, advancing the understanding of their potential in marine CO_2 storage applications.

2. Materials and Methods

2.1. Equipment and materials

The experimental setup is formed by a high-pressure reactor, connected to a CO_2 gas cylinder and controlled by a chiller (Fig. 1). The reactor, made of 316 stainless steel (316SS), was designed for pressures up to 150 bar and has an internal volume of 949 cm^3 , with an inner diameter of 0.073 m and an internal length of 0.023 m. The width of its walls is 0.0076 m and it is closed by two enclosing plates (width 0.047 m). The reactor is equipped with several ports for gas flow and instrumentation: a gas inlet valve is located at the bottom flange, while an outlet/purge valve is mounted on the top flange. Temperature is measured using four Class 1 precision K-type thermocouples, which are called T02, T07, T11, and T16, since they are placed respectively at 2 cm, 7 cm, 11 cm and 16 cm from the upper flange. Pressure is measured using a digital manometer (Model MAN-SD). All data from sensors are recorded by a data acquisition system. To maintain stable

Table 1
Hydrate formation parameters (PW = pure water; PW+S= pure water + sediment).

No.	Type	Pi form	Ti form	Pf form	Tf form	Pi diss	Ti diss	Pf diss	Tf diss	n_{CO_2}	n_{CO_2hyd}	G.U. (%)	ρ_{form} (kg/m^3_{H2O})	ρ_{form} (kg/m^3_{sand})	W.C.R. (%)
1	PW	34.56	3.16	17.97	2.19	0.24	2.19	5.98	9.21	1.63	0.13	7.73	11.71	-	2.87
2	PW	33.47	5.81	22.11	5.71	0.51	5.71	3.25	13.57	1.15	0.06	4.99	5.34	-	1.31
3	PW	25.13	1.79	21.57	2.24	0.7	2.24	5.5	10.11	0.67	0.10	15.57	9.71	-	2.38
4	PW	25.13	1.59	21.57	2.14	0.89	2.24	6.4	10.21	0.67	0.12	18.21	11.36	-	2.79
5	PW+S	35.3	3.89	32.51	1.99	0.3	0.89	6.22	14.31	0.62	0.06	9.70	23.41	5.58	5.51
6	PW+S	33.01	6.46	22.15	5.24	0.3	0.04	6.04	12.22	0.38	0.04	11.46	17.14	4.09	4.03
7	PW+S	25.95	1.57	13.7	0.21	0.1	3.63	9.89	11.37	0.25	0.09	36.68	36.14	8.62	8.50
8	PW+S	22.0	1.84	16.69	0.1	0.4	1.66	8.75	11.57	0.20	0.06	31.87	25.38	6.05	5.97

thermal conditions, the entire reactor is located inside a thermostatic bath containing a water-glycol mixture. Temperature inside the bath is regulated using a circulating chiller (Model GCLT, Eurochiller), which can reach temperatures as low as −30 °C. Figs. 1 and 2 illustrate the schematic diagram of the setup and pictures of the gas bottles, reactor and chiller.

CO_2 is supplied by Nippon Gases and has a purity grade of 99.95%. Pure distilled water was used for hydrate formation, while natural sand was taken from the Adriatic Sea. For the experimental tests, the reactor was filled with natural sand for 50% of its volume (474 cm^3) and then mixed with distilled water so that the sand is fully saturated with water.

So, the experimental apparatus realizes the CO_2 injection from the bottom flange into the fully water-saturated porous medium. Under these conditions, the injected gas distributes in the sediment and progressively invades the connected pore network.

2.2. Experimental procedure

This study investigated CO_2 hydrate formation and dissociation in two different systems: binary system, with just gas and pure water and a three-phase system, with gas, water and natural sand. The experiments were carried out considering different values of initial temperature and pressure, as summarized in Table 1.

The main objective was to compare the two different systems to highlight the effect of the natural sand on CO_2 hydrate formation under varying thermodynamic conditions. The procedure began with cooling the reactor to a targeted initial temperature. Once the target temperature was reached, CO_2 was introduced into the reactor until the desired initial pressure was achieved.

Hydrate formation then started and proceeded in isochoric conditions. The starting point of the hydrate formation was identified by a sudden pressure drop and a slight temperature increase due to the exothermic nature of the reaction.

Once hydrate formation was complete, the reactor was gradually depressurized and the cooling system was turned off, allowing the temperature to rise beyond the equilibrium point. This led to the dissociation of CO_2 hydrates, during which the total volume of gas released was measured to determine the amount of gas previously trapped in the hydrate structure. During the dissociation phase, additional analyses were performed on selected tests, chosen based on the presence or absence of sediment and on different pressure conditions. In particular, two indicators were evaluated to enable a consistent comparison of dissociation behaviour: the average dissociation rate during the first 60 min and the fraction of CO_2 released over time. The average dissociation rate represents the amount of CO_2 released per unit time in the initial stage of dissociation, providing an estimate of how fast the process occurs. The fraction of CO_2 released was defined as the percentage of the total dissociated CO_2 that is released within a given time interval, with particular focus on the first 60 min. This parameter allows assessing the extent of dissociation relative to the total amount of hydrate formed. The analysis of the dissociation stage under unconfined conditions was performed to assess the intrinsic stability of the formed hydrates in response to thermal perturbation. Therefore, this approach is not intended to reproduce long-term geological stability. CO_2 hydrates in water were also formed to take samples for microscopic investigations described in Section 2.3.

The initial and final values of temperature and pressure during both hydrate formation and dissociation were used to calculate key thermodynamic and kinetic parameters, as described below.

2.2.1. Total Moles of CO_2 Gas Injected into the Reactor

The total number of CO_2 moles injected is given by the ideal gas law with compressibility correction as in Eq. 1:

$$n_{CO_2} = \frac{P_{i,form} \bullet V_{freegas}}{Z_{i,form} \bullet R \bullet T_{i,form}} \tag{1}$$

2.2.2. Total Moles of CO_2 Gas Encapsulated in Hydrate Form

The amount of CO_2 captured in the hydrate form is calculated as in Eq. 2:

$$n_{CO_2hyd} = \frac{V_{free\ gas}}{R}\left(\frac{P_{f,diss}}{Z_{f,diss} \bullet T_{f,diss}} - \frac{P_{i,diss}}{Z_{i,diss} \bullet T_{i,diss}}\right) \tag{2}$$

2.2.3. Gas Uptake

The percentage ratio of the amount of CO_2 captured in the hydrates to the total number of moles of CO_2 injected into the reactor is given in Eq. 3:

$$G.U. = \frac{n_{CO_2hyd}}{n_{CO_2}} \bullet 100 \tag{3}$$

2.2.4. Formation Density

The CO_2 amount stored in the hydrates per unit volume of water is given by Eq. 4:

$$\rho_{form} = \frac{n_{CO_2hyd} \bullet PM_{CO_2}}{V_{H2O}} \tag{4}$$

For sand-containing systems, an alternative definition of formation density can be introduced by normalizing the amount of CO_2 stored in hydrates to the volume of sand, replacing V_{H2O} with V_{sand}. This definition provides a metric more representative of storage in porous media and allows a more direct comparison with geological storage capacities.

The comparison between systems with and without sand is consistently performed using formation density normalized to the water volume, in order to ensure a consistent evaluation of the sediment effect under comparable conditions.

2.2.5. Water conversion rate

The percentage ratio of water converted to hydrates and the total amount of water in the reactor is calculated as in Eq. 5:

$$W.C.R. = \frac{n_{CO_2hyd} \bullet N_{hyd}}{V_{H2O} \bullet \rho_{H2O}/PM_{H2O}} \bullet 100 \tag{5}$$

Where

$P_{i,form}$ and $P_{f,form}$ – The initial and final Pressures of formation, respectively.

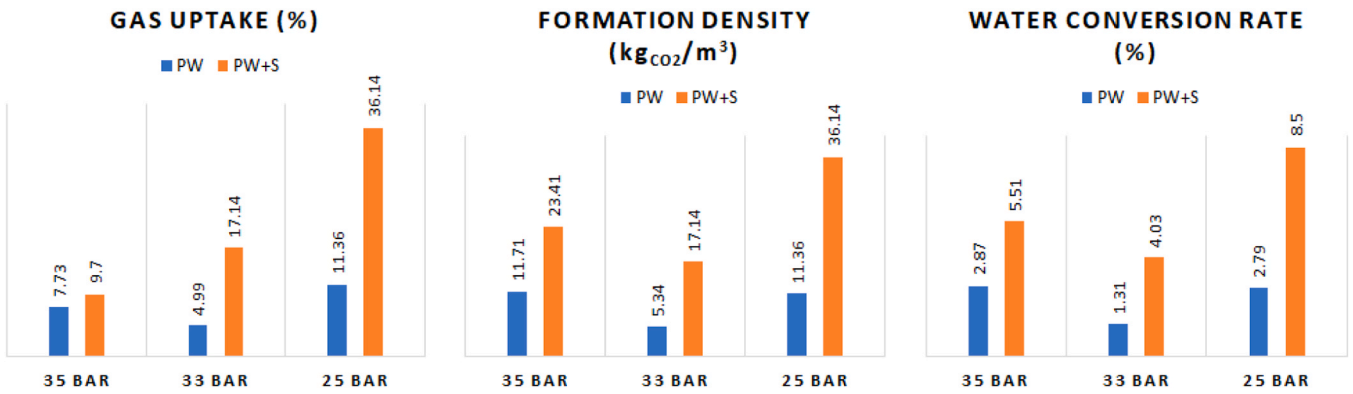

Fig. 3. Effect of sediment on CO_2 hydrate formation at different pressures. Comparison of gas uptake, formation density, and water conversion rate between pure water (PW) and sediment-containing (PW+S) systems at formation pressures of 35, 33, and 25 bar.

$T_{i,form}$ and $T_{f,form}$ – The initial and final Temperatures of formation, respectively.

$P_{i,diss}$ and $P_{f,diss}$ – The initial and final Pressures of Dissociation, respectively.

$T_{i,diss}$ and $T_{f,diss}$ – The initial and final Temperatures of Dissociation, respectively.

$Z_{i,diss}$ and $Z_{f,diss}$ – The compressibility factor was calculated using the Peng-Robinson equation of state at the initial and final temperature and Pressure values of Dissociation, respectively.

$V_{free\ gas}$ – Volume of free gas inside the reactor.

V_{H2O} – Volume of water inside the reactor.

V_{sand} – Volume of sand inside the reactor.

ρ_{H2O} - Density of water.

R- Universal gas constant.

PM_{CO_2} - Molecular weight of CO_2.

PM_{H2O} – Molecular weight of water.

N_{hyd} – Hydration number (5.75).

The key parameters for each test are reported in Table 1.

2.3. Microscopic characterization: FE-SEM and BET measurements

The natural sand, sampled on Adriatic Sea has been morphologically characterized by Field Emission Scanning Electron Microscopy (FE-SEM, Sigma 300, Zeiss) operating at 20 kV, equipped with Energy Dispersive X-ray spectroscopy (EDX, Quantax, EDS, Bruker).

The sample was deposited on aluminium stabs using self-adhesive carbon, dried in vacuum oven (Vismara, 65) at 80 °C. To prevent charging during the analysis, the sand sample was sputter with chromium (5 nm) by Quorum Q150T-ES (Quorum Technologies, Lewes, UK).

The porosity and the total volume of the pore of the natural sand was measured by BET measurements through volumetric N_2 adsorption at – 195.8 °C using an ASAP 2020 (Micrometrics) instrument. The BJH method (Halsey thickness equation) was used to evaluate the porosity of the natural sand material.

The collected CO_2 hydrates, produced in the equipment described in Section 2.2, were analysed using a scanning electron microscope (Field Emission SEM, Sigma 300, Zeiss) coupled with a temperature-controlled equipment (Coolstage by Seben) that permits to acquire images up to –30 °C. The CO_2 hydrates, once formed, were immediately placed in a sample holder immersed in liquid nitrogen. The holder containing the frozen hydrates was then transferred to the pre-cooled SEM stage using cryogenic handling procedures to avoid any temperature rise during transfer. Imaging was performed under very low temperature (−30 °C) and low-pressure conditions.

2.4. Raman analysis on pure water samples with and without sand and CO_2 gas hydrates

Raman analysis on pure water with and without sand has been operated using a Horiba iHR-320 Raman spectrometer coupled with an Olympus microscope using a green laser (532 nm line, 30 mW). For the measurements a 50 × microscopic objective (NA = 0.50) was used, in order to focus the laser beam (5 μm in diameter) onto the sample and to collect the Raman photons produced by the sample in backscattering configuration.

The Raman spectrometer works also with a Linkam THMS600 commercial microscope stage which allowed to operate at different temperatures (ranging from – 195 °C to 600 °C). The total acquisition time for each spectrum was 150 s using 600 g/mm grating. Different temperatures have been evaluated: 1, 2, 3 and 6°C, and below zero from – 10 to – 60°C. At each temperature the Raman spectrum was acquired from multiple points (n = 4) on the sample surface, and each spectrum was pre-processed (baseline correction, normalization) using the same protocol.

In addition, the CO_2 gas hydrates prepared, as explained in Section 2.2, using pure water with and without sand, have been also characterized by Raman analysis, at – 60°C, to confirm the uptake of CO_2 analysing the presence of the CO_2-diad Fermi peaks. Also in this case, the Raman spectrum of CO_2 hydrates was acquired in multiple points on the sample surface (n = 4).

3. Results and discussion

In this section, the results of the CO_2 hydrate formation process and the microscopic investigation are presented.

3.1. Hydrate formation and dissociation tests

Table 1 summarizes the experimental parameters and results related to the formation and dissociation tests. The experimental campaign is formed by 8 experimental tests: Tests 1–4 are carried out in binary system (just water and gas), while Tests 5–8 are carried out in presence of natural sand with water and gas. The analysed pressure range is 25–35 bar, with three approximate pressure levels investigated (25 bar, 33 bar and 35 bar), both in binary and three-phase systems.

The use of natural quartz-rich sand, full water saturation and operating pressures in the range of 22–35 bar are conditions representative of shallow marine sandy sediments, such as those typically found in continental shelf and upper slope environments. The results based on a comparative approach, aimed at isolating the effect of sandy sediments under controlled conditions, rather than reproducing the full complexity of natural geological systems.

In addition, the selected pressure range corresponds to marine

conditions, where pressure–temperature couples are close to the hydrate equilibrium boundary. This region is particularly relevant from an application perspective, as it represents a critical zone where hydrate stability is more sensitive to environmental perturbations.

Comparing binary systems (Tests 1–4, PW) to the three-phase systems (Tests 5–8, PW+S), one of the critical observations in this study is the general increase of the performance parameters, which means an improvement of hydrate formation in porous media. As presented in Table 1, gas uptake values in sediment systems (Tests 5–8) range from 9.70% to 36.68%, significantly higher than the range 4.99–18.21% observed in pure water (Tests 1–4). Also formation density and water conversion rate are notably higher in three-phase systems. The highest formation density recorded is 36.14 kg/m^3 with sediment (Test 7), compared to 11.71 kg/m^3 in pure water (Test 4), while water conversion rates reaches 8.50% (Test 7) in sediments and 2.87% in pure water (Test 1). These results suggest that the presence of natural sand enhances hydrate formation and storage capacity, if compared to the binary system.

Fig. 3 shows the results to better highlight the effect of the sediment on CO_2 hydrate formation at different pressures. The presence of the natural sand (PW+S in Fig. 3) always enhances gas uptake, formation density and water conversion across all pressure levels tested.

At an initial pressure of 35 bar, gas uptake passes from 7.73% in binary system to 9.70% obtained with sand, while formation density nearly doubled (from 11.71 to 23.41 kg_{CO2}/m^3). At 33 bar, the improvement is even more pronounced, with gas uptake increasing from 4.99% to 17.14%, together with a substantial increase also in formation density and water conversion rate. The most significant improvement occurs with 25 bar, where tests in presence of sand achieve a gas uptake of 36.14% and a water conversion rate of 8.50%, compared to only 11.36% and 2.79% in pure water respectively. These results clearly demonstrate that sediment acts as a strong promoter of hydrate formation. The enhancement effect becomes more prominent at lower pressures, compensating for the reduced thermodynamic driving force and therefore indicating its conversion-driven promoting role.

In fact, as underlined by [15], gas hydrates start to form at the gas-water interface: higher is this interface extension, higher will be the hydrate content at the same stability conditions. Moreover, high water saturation of the sample promotes the hydrate formation. These considerations suggested that in our samples before the hydrate formation: i) the pores are connected and fully water saturated; ii) the pore shape favors the high interface gas-water; iii) the free gas is uniformly distributed in the pore sediments.

So, the sediment improves the effectiveness of gas–water interaction and reduces transport limitations, allowing a larger fraction of water to be converted into hydrate under the same operating conditions. This behaviour can be interpreted as an enhancement of the conversion efficiency, reflecting a more efficient utilization of the sediment volume.

While the system represents a simplified analogue of natural marine sediments, it captures the key pore-scale mechanisms governing hydrate formation, including distributed gas–water interfaces, heterogeneous nucleation and confined growth within the porous medium.

The formation densities of CO_2 hydrates obtained in the experimental campaign can be interpreted using two different reference volumes. When normalized to the water volume, the maximum value reaches 36.14 kg/m^3, reflecting the efficiency of hydrate formation. However, for comparison with geological storage systems, formation density should be referred to the sediment volume. In this case, the maximum value obtained is 8.62 kg/m^3.The density of CO_2 storage within a reservoir, measured in kilograms of CO_2 per cubic meter of reservoir volume, varies significantly based on the storage mechanism. When CO_2 is dissolved in water, storage densities range from about 4–13 kg/m^3 . Mineralized CO_2, which forms solid carbonates over time (typically within 10–100 years), can achieve densities between 30 and 200 kg/m^3 . The highest densities, ranging from 50 to 240 kg/m^3 , are seen with supercritical or liquid CO_2 injected in depleted oil reservoirs,

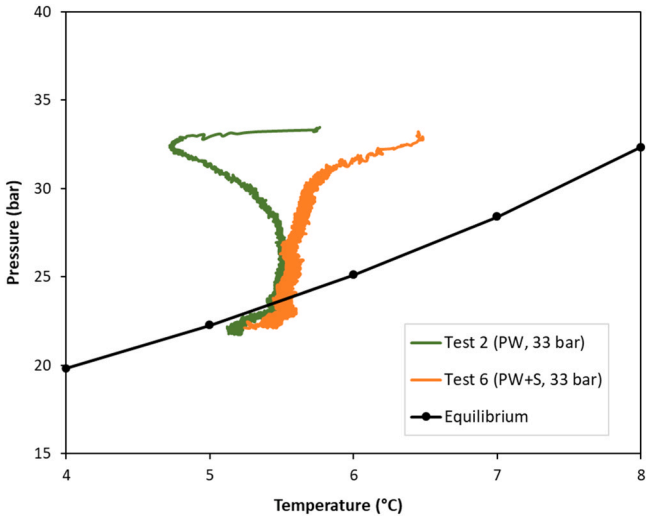

Fig. 4. Pressure-Temperature profiles during the for PW (Test 2) and PW+S (Test 6) systems compared with the equilibrium curve.

which allows the most compact storage but also carries a higher risk of leakage compared to other phases [16]. In comparison, CO_2 hydrates formed in situ within porous marine sediments represent a diffuse storage mode, with moderate storage densities but potentially high geomechanical stability [17], and faster formation timescales than mineralization under favorable thermodynamic conditions, as hydrate crystallization occurs within minutes to hours once pressure and temperature enter the stability zone, whereas mineral carbonation reactions typically require weeks to years to achieve comparable CO_2 fixation [18].

Another consideration, which can be done, is on the effect of temperature both with and without sediment. To isolate the influence of temperature on CO_2 hydrate formation, comparisons were made among experiments conducted at similar pressure levels. At the 25 bar (Tests 3 and 4), the test performed at the lower temperature (T_{iform} = 1.59°C) achieved a higher gas uptake (18.21%) and formation density (11.36 kg/m^3) than the test at a slightly higher temperature (T_{iform} = 1.79°C, G.U. = 15.57%, ρ_{form} = 9.71 kg/m^3). A similar trend is observed in presence of the natural sand. Even though at slightly lower pressure (Tests 7 and 8), the initial temperature decrease from 1.84°C to 1.57°C leads to a substantial increase in gas uptake (from 31.87% to 36.68%) and water conversion (from 5.97% to 8.50%). This confirms that, even in the presence of sediment, the formation process is strongly temperature-dependent.

A replicability analysis of the tests reported in Table 1 was performed on Test 2 (PW, 33 bar), Test 3 (PW, 25 bar), Test 6 (PW+S, 33 bar) and Test 7 (PW+S, 25 bar). For each test, the coefficient of variation (CV) was calculated for gas uptake, formation density and water conversion. For PW at 25 bar, CV values are approximately 11–12%, while at 33 bar they range between 4% and 8%. For sediment-containing systems (PW+S), CV values are approximately 3–8% at low pressure and 11–15% at higher pressure. Overall, CV values are generally below 15%, indicating acceptable reproducibility of the experimental data. Importantly, the identified enhancement of gas uptake, formation density and water conversion in the presence of sand is consistently confirmed across comparable conditions.

Gas hydrate formation is an exothermic process, releasing heat during nucleation and growth [4]. This heat release is evident in temperature measurements during hydrate formation, with significant spikes observed in pure water systems, as illustrated in Fig. 4. The figure compares the formation curves in pure water (Test 2 in Table 1) and sediment-containing systems (Test 6 in Table 1), highlighting a noticeable temperature increase in the pure water system due to the absence of

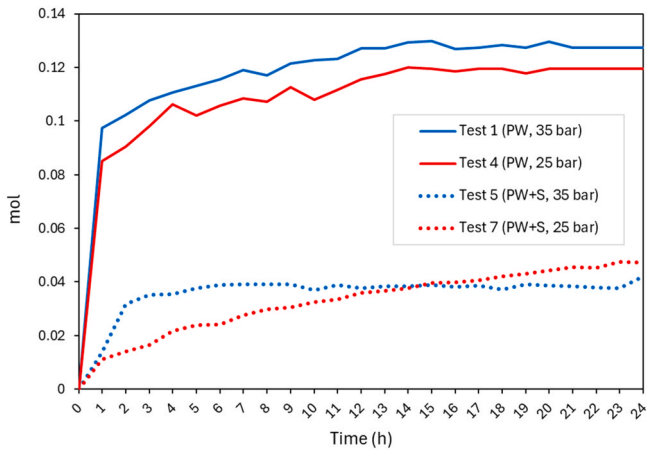

Fig. 5. Temporal evolution of the dissociated moles comparing PW and PW+S systems at two different values of pressure.

heat dissipation mechanisms. In contrast, in presence of sediment, the temperature increase is negligible due to the thermal absorption and distribution of nucleation sites within the sediment matrix [13]. By preventing the development of local thermal hotspots, the sediment effectively reduces the likelihood of partial hydrate dissociation caused by localized overheating. This, together with the presence of heterogeneous nucleation sites, which reduce the energy barrier for nucleation [19], explains the global promotion of the sediment.

So, sediments modify the local environment, providing heterogeneous nucleation points and heat dissipation. The increased occurrence of nucleation points promotes a more spatially distributed hydrate formation. At the same time, improved heat dissipation mitigates local temperature increases associated with the exothermic formation process, maintaining favourable conditions for hydrate growth. Collectively, these effects enable enhanced hydrate formation (higher formation density and water conversion rates) even under reduced thermodynamic driving forces, as evidenced by the experimental results. This is consistent with other literature results, as reported in (Wang L. et al., 2022)[5].

While CO_2 hydrate formation is enhanced by the presence of the sediment, its effect on dissociation consists in a global delay of the process, especially in the initial stage. Fig. 5 shows the cumulative moles of CO_2 released during dissociation for PW and PW+S systems under two different values of pressure: 35 bar (Tests 1 and 5) and 25 bar (Tests 4 and 7). A rapid initial increase is observed in all cases during the first hours, then the dissociation process slows down. A significant difference between PW systems and PW+S systems emerges in the early stage of dissociation. In the first hour, PW systems release a significantly larger fraction of CO_2, reaching 75% in Test 1 and 70.9% in Test 4 of the total CO_2 amount in the hydrate phase, whereas PW+S systems release 23.2% in Test 5 and 12.4% in Test 7 over the same time interval. This difference indicates that the presence of sand delays the hydrate dissociation.

After 24 h, the CO_2 dissociation is almost complete in PW systems (98.1% in Test 1and 99.7% in Test 4), while in PW+S systems, the percentage amount of dissociated CO_2 moles reaches 64.3% in Test 5 and 49.1 in Test 7, indicating that dissociation remains slower in the presence of sand. This interpretation is further supported by the evaluation of the average dissociation rate in the first 60 min $(dn/dt)_{0–60min}$. For PW systems, values of $1.6{\cdot}10^{-3}$ mol/min and $1.4{\cdot}10^{-3}$ mol/min are observed respectively in Test 1 and Test 4, whereas in PW+S systems, the rate is one order of magnitude lower ($2.3{\cdot}10^{-4}$ mol/min in Test 5 and $1.9{\cdot}10^{-4}$ mol/min in Test 7). This behaviour is consistent with previous literature findings, such as thos reported in [20]. In their study, quartz sand with particle size lower than 600 μm, comparable to the sand used in the present work, showed the lowest rate of CO_2 release compared to other coarser systems. The observed slower dissociation in the presence of sand can be attributed to the combined influence of capillary effects and heat transfer limitations connected to the grain size, as discussed in [20]. Free dissociation, although different from natural conditions, provides a useful framework to identify the intrinsic effects of the porous medium.

However, under pressurized geological conditions, the sediment matrix would be expected to slow hydrate decomposition due to limited heat and mass transport. In such environments, the released gas cannot readily escape, and the retained pore pressure acts as a thermodynamic buffer that keeps the system near the hydrate stability boundary, thereby enhancing the long-term stability of CO_2 storage.

3.2. Sand characterization

Scanning Electron Microscopy was employed to study the surface morphology of marine sand used in the hydrate formation and dissociation tests in Table 1.

Fig. 6a shows the surface structure exhibiting a dense and clear microstructure, while the zoom of one particular of this sand (Fig. 6b) describes that the surface is not regular but shows a grade of porosity.

In addition, EDX analysis in different regions of the sample, as reported in Fig. 7, demonstrate large presence of Si that could be attributed primarily to the pure silica (quartz) composition of this sand, while the presence of Ca could be attributed to the presence of $CaCO_3$ salt; in addition, minor elements have been detected, as Mn, Fe, K and Cr, the latter due to the metallization of the samples.

The nitrogen adsorption-desorption isotherm showed a shape typical of the IV isotherms with a distinct hysteresis loop at a relative pressure p/p° between 0.4 and 1, indicating a material dominated by mesopores and slit-like intergranular voids [21]. The Brunauer-Emmett-Teller (BET) surface area and the total volumes of the pores for the natural sand sample, are 1.5099 m^2 /g and 0.003803 cm^3/g, respectively. The average pore diameter is about 16 nm (BJH adsorption). A minor contribution from micropores (< 2 nm) was detected, with a micropore volume of 1.46×10^{-4} cm^3 /g and a micropore area of 0.34 m^2/g, indicating that the material is primarily mesoporous with limited

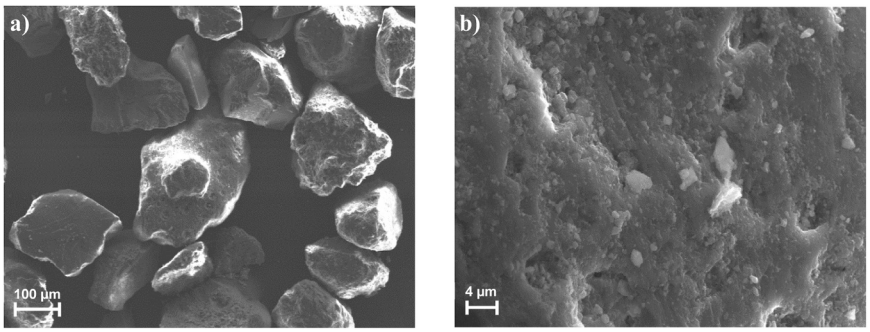

Fig. 6. SEM images of natural sand at different magnification a) 290 × and b) 5 K× .

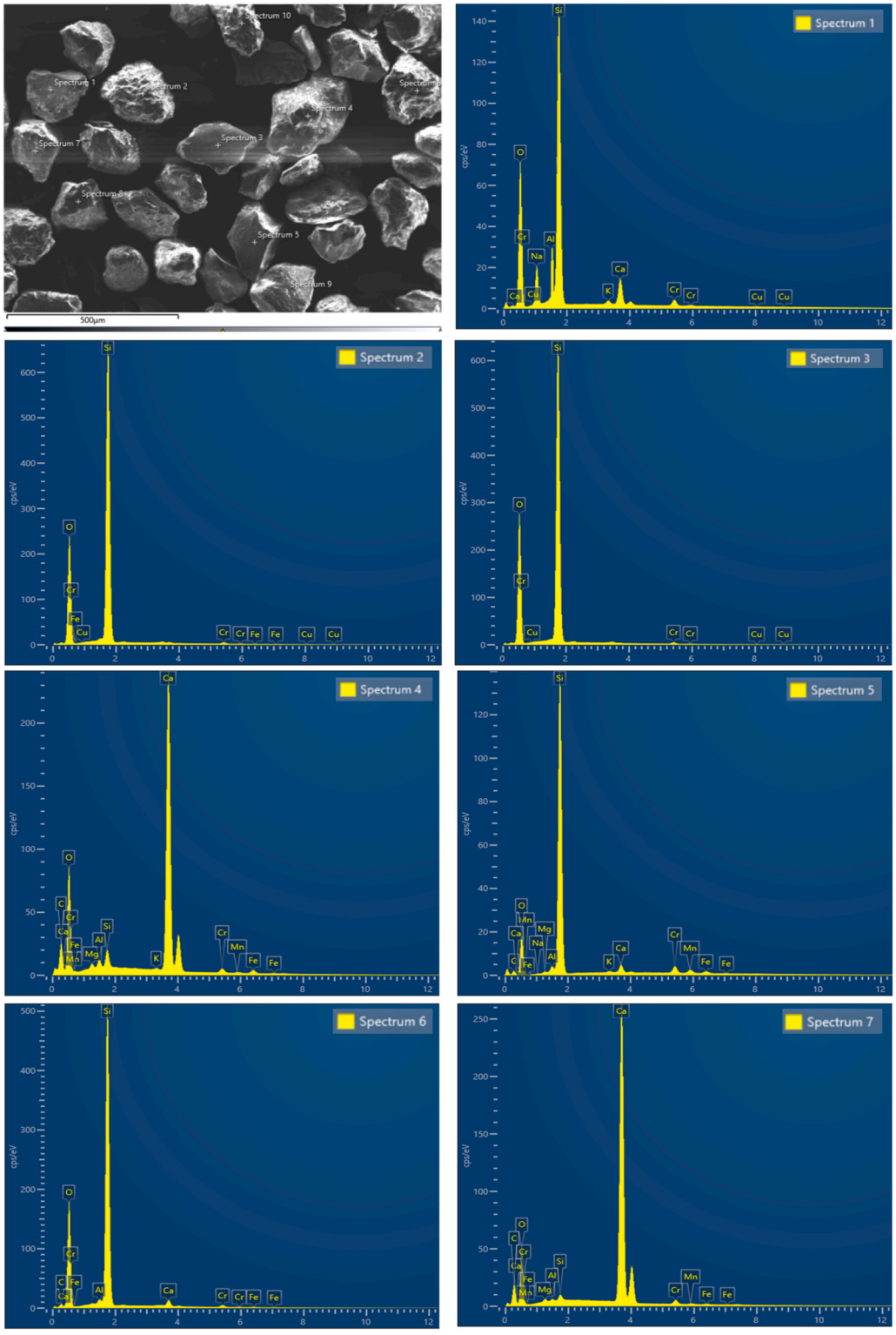

Fig. 7. EDX analysis of natural sand sample.

microporosity.

This porous structure promotes heterogeneous nucleation and gas–liquid interfacial contact, enhancing CO_2 hydrate formation kinetics. The mesopores facilitate molecular diffusion and localized gas enrichment, while the limited microporosity and surface asperities observed in SEM images in Fig. 6 likely provide nucleation sites. This structural arrangement explains the higher gas uptake, formation density, and water conversion rate measured in sediment-containing systems (Tests 5–8, Table 1), compared to the pure water system.

The natural sand used in this study is representative of sandy marine sediments typically found in continental shelf and upper slope environments, where permeable sand-dominated layers are present. However, marine sediments can exhibit significant variability, including clayey-silt deposits characterized by finer grain size, higher clay mineral content and reduced permeability, such as those described for the Shenhu area, China [30]. In this investigation, hydrate formation is

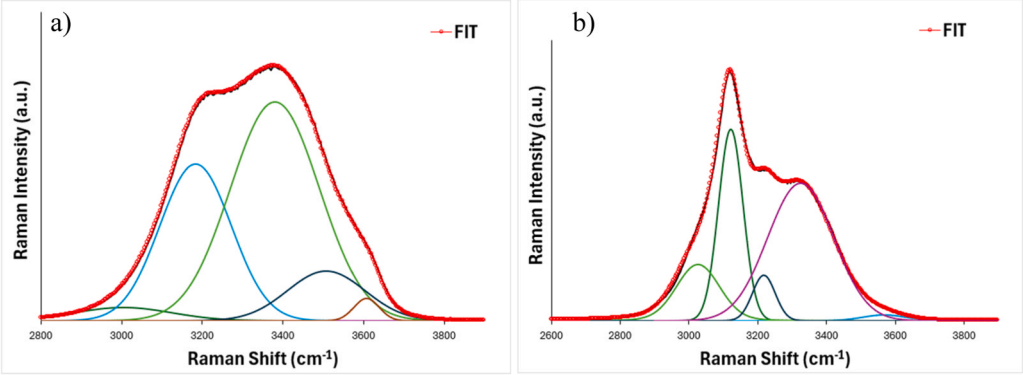

Fig. 8. Raman spectra of a) liquid water (3°C) and ice water (– 60°C).

Table 2
Raman shifts of pure water at 3°C and – 60°C.

	Liquid water (°3 C)	Ice water (– 60°C)
DAA-OH	3303.24	3025.01
DDAA-OH	3198.41	3120.05
DA-OH	3386.88	3217.12
DDA-OH	3517.51	3325.59
Free-OH	3610.3	3568.1

governed by a dynamic coupling between hydrate growth and sediment migration: hydrates initially form at the gas–liquid interface, followed by particle migration and aggregation at the interface, which can temporarily hinder gas–water contact and lead to a plateau in hydrate formation. Subsequent formation of capillary channels enables renewed gas–water interaction and further hydrate growth through a feedback mechanism. In contrast, the natural sand investigated in this study forms a static, permeable porous framework, where hydrate formation is controlled by distributed gas–water interfaces within the pore network. This difference reflects two distinct hydrate formation regimes, arising from the general physical characteristics of the sediment.

3.3. *Raman analysis on pure water samples with and without sand and CO_2 gas hydrates*

Gas hydrates are composed by water molecules that arrange themselves to form polyhedron cage with specific structure interacting by hydrogen bonds. Raman spectroscopy, in this context, is an important technique to characterize gas hydrates and also to investigate the interaction of water molecules by hydrogen bonds, studying the characteristic stretching vibrations of water molecules in the range between 2700 and 3800 cm^{-1}. The analysis of these bands permits to evaluate and study the parameters that affect the hydrogen bonds, modifying the inter-molecular coupling of symmetric and asymmetric -OHs stretching vibrations, giving important information about structure, dynamic properties of water and its phase. Water molecules can interact together

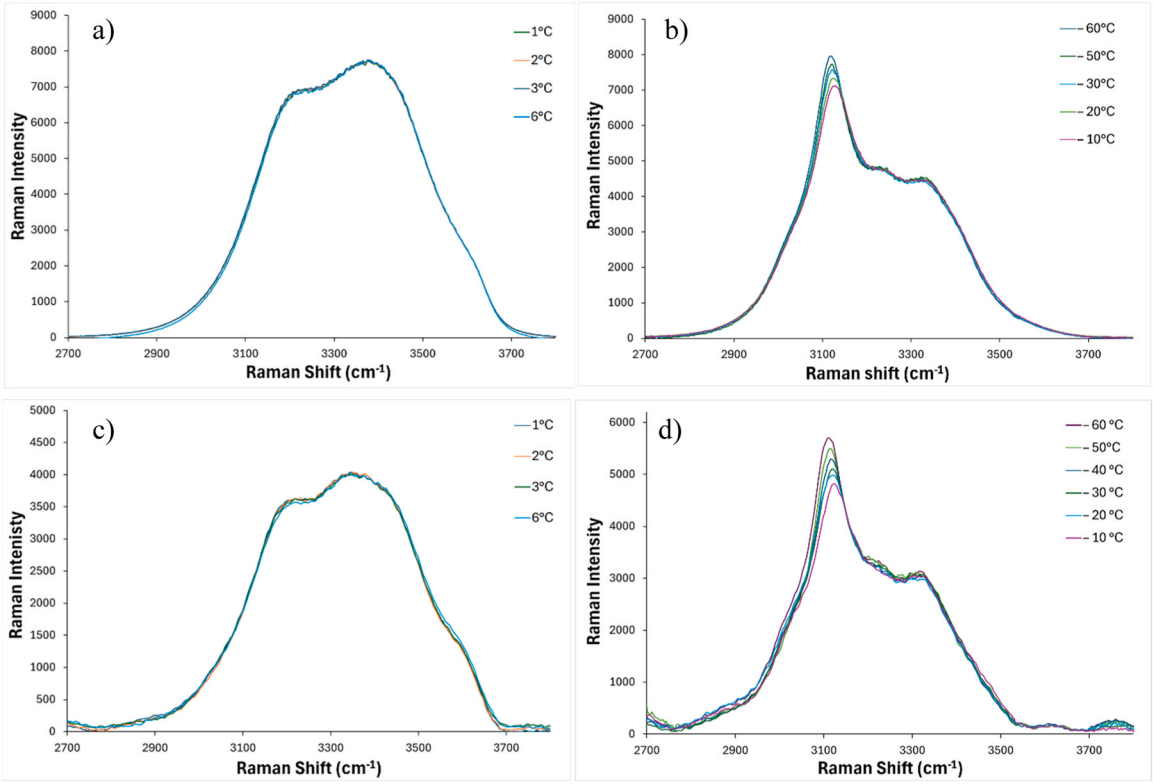

Fig. 9. Raman spectra of water molecules vibrations (a,b) without and (c,d) with sand sediments at different temperatures: above zero (left) and below zero (right).

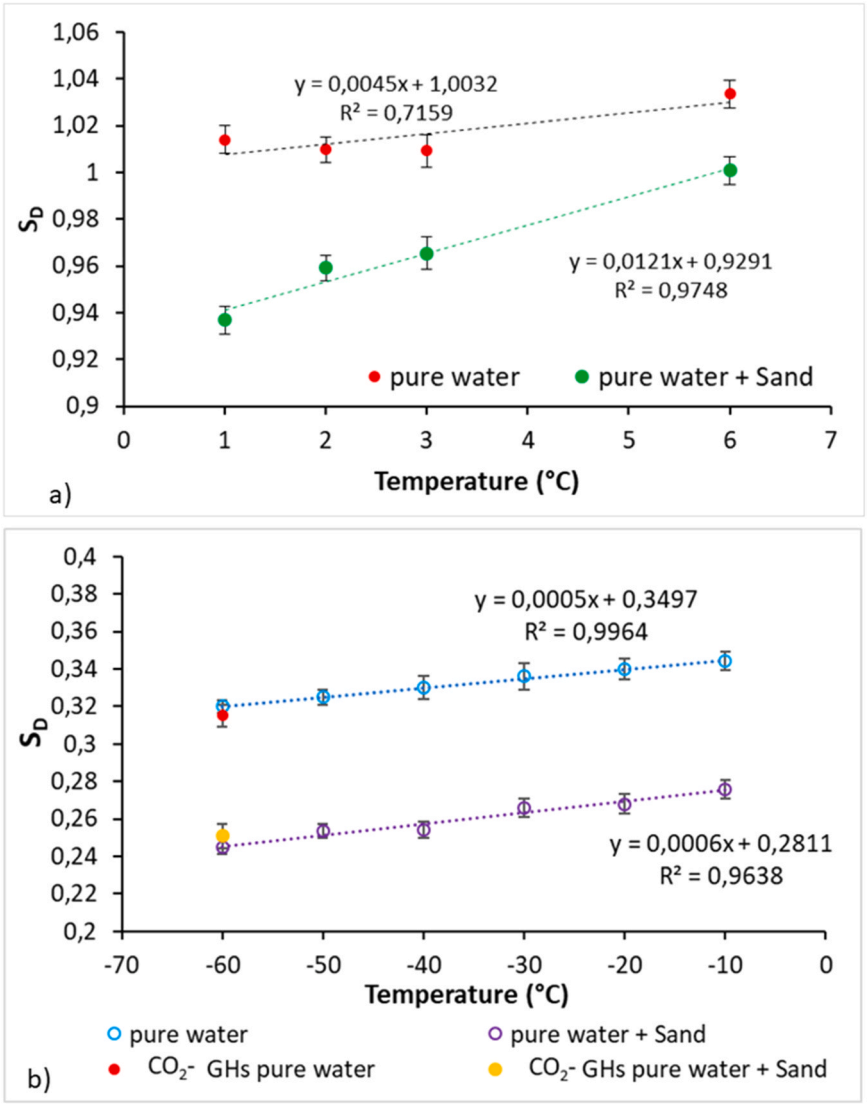

Fig. 10. Correlation of S_D index as function of change in temperatures for a) pure water and b) pure water with natural sand samples.

by hydrogen bonds as proton donor (D), proton acceptor (A) and their combination; for these considerations, the Raman -OHs stretching vibrations of water can be divided in five different contributions: DDAA-OH, DDA-OH, DAA-OH, DA-OH and free OH, respectively [22–24], as reported in Fig. 8.

The liquid water shows two main bands at 3188.41 and 3386.88 cm^{-1}, the Raman spectrum of ice water shows an intense peak at 3120.05 cm^{-1}, showing that the region below 3200 cm^{-1}, relative to the symmetric stretching vibrations, increase, while the region above 3200 cm^{-1}, responsible for the asymmetrical stretching vibration, strongly reduced in intensity (Fig. 8). This behaviour can be explained because in the ice form, due to the water expansion and stability, the vibrational modes are reduced; on the contrary in the liquid phase, the asymmetrical contributions are more intense due to the flexible structure of water. The Raman shifts and the main bands of liquid water and ice are summarized in Table 2.

The Raman spectra of pure water and pure water with sand were explored at positive temperatures in the range 1–6 °C to obtain information related to water band at the starting points related to gas hydrate formation. In this case, the observation of -OHs bands permits to define the organization of the water molecules investigating the asymmetric and symmetric stretching of the different types of bands and the relative influence of sand. The Raman spectra of liquid water with and without natural sand are reported in Fig. 9(a,c).

The Raman spectra of the liquid water with and without natural sand shows the same spectral features as function of temperature; in that case, a small increase of the asymmetric stretching bands (below 3300 cm^{-1}) occurred when the temperature decreased and approached near to 0°C.

In addition, since ice water presents similarity with gas hydrates [31], Raman measurements of ice water and ice water with natural sand, from –10 to – 60°C, were performed to obtain information about the influence of sand sediments and temperature on the hydrates structure and their formation.

The Raman spectra of ice with and without natural sand are reported in Fig. 9(b,d); from the spectra is possible to observe that, at higher temperature, the region of the symmetric stretching vibrations (below 3300 cm^{-1}) decreased and shifted at higher frequencies, indicating that, the increased temperature produced a decrease of the symmetric -OHs bands. A slight shift to higher frequency was observed for the asymmetric bands. The spectral variations are similar with and without natural sand.

To obtain information from all the samples analysed by Raman spectroscopy, the ratio between the areas of the symmetric and asymmetric stretching of -OHs, in the range between 2800 and 3800 cm^{-1}, were calculated [25]. The areas of the two regions were obtained by the determination of the isosbestic point at 3325 cm^{-1}, that divided the

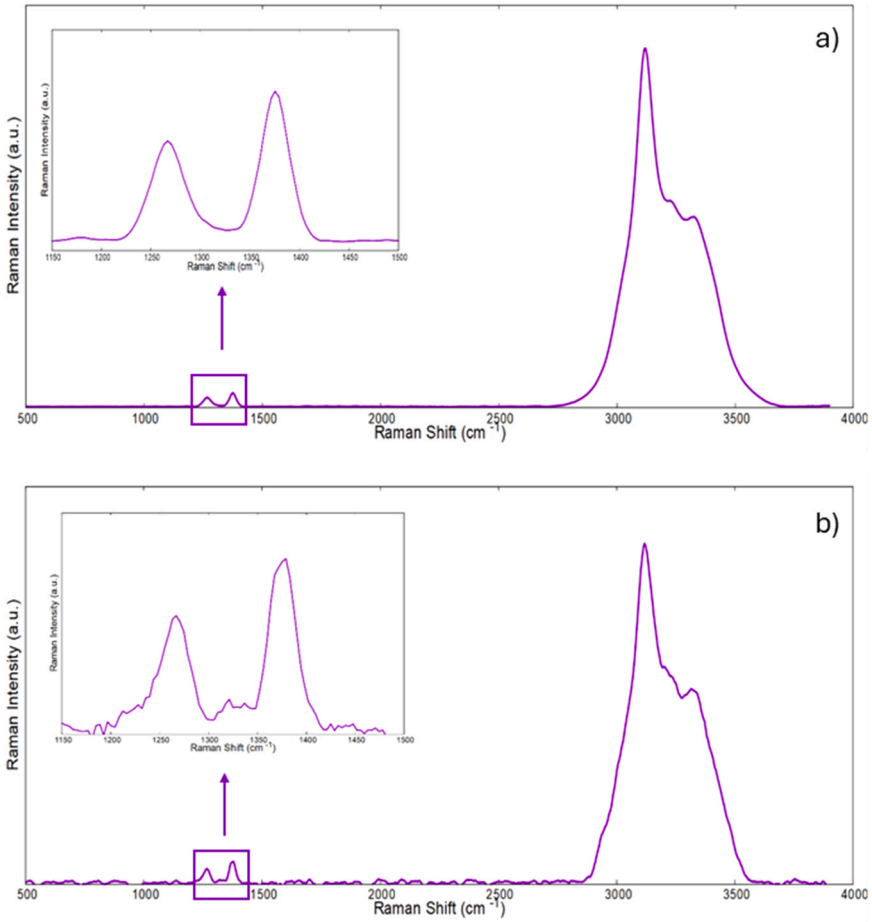

Fig. 11. Raman spectra of CO_2 hydrates, recorded at – 60°C, in (a) pure water and (b) pure water with natural sand, showing the CO_2 Fermi- peaks (insert of figures) and -OHs bands of water molecules.

-OHs stretching band in two regions, the A region, associated to the symmetric -OHs bands of water, and B region for the asymmetric bands of -OHs water molecules. The two areas, for each Raman spectra, for pure water and pure water with natural sand, at different temperatures, were then determined and the ratio between the two regions (B/A), that represents the S_D index, was calculated [25–27]. The Raman spectra were acquired in multiples point on the sample surface; the S_D index with standard deviations at different temperatures for liquid water and ice with and without natural sand are reported in Fig. 10(a,b).

In the case of liquid water, the S_D index, as reported in the plot of Fig. 10a, for pure water is higher than those with sand showing an increase with temperatures values; high linear correlation for pure water with natural sand was obtained. This result shows that the sand organized the structure of water, with an increase of symmetric vibrations contribution at lower temperatures. This trend correlates with the hydrates formation; in fact, at the temperature values where the structure is more organized (lower S_D index), reflecting lower disorder, the hydrates formation is higher as demonstrated by the higher water conversion rates at lower initial temperatures (Ti) of formation (Table 1).

Plotting the S_D index of ice water (Fig. 10b), it is possible to observe a direct correlation with the increase of temperature for both the ice water with and without natural sand.

Analysing this trend, it can be observed that the symmetric stretching contribution of the -OHs bands is higher in presence of natural sand (lower S_D), as compared to that without sand (higher S_D); the presence of sand, probably due to the interaction of the silanol groups (Si-OH), by hydrogen bond, with water molecules, provided a more ordered structure. This result, also in this case, is in accordance with the higher water conversion efficiency and density formation in presence of sand, reported in Table 1.

In addition, the parallel line of the S_D index vs Temperature of Fig. 10b, confirms that the stability of ice water was affected in the same way with and without natural sand.

Finally, the CO_2 hydrates in pure water with and without natural sand have been analysed by Raman spectroscopy (Fig. 11 a,b); in both cases, it is possible to detect the characteristic Fermi-diad peaks of CO_2 in the hydrate structure: the stretching vibration C–O ($\nu 1$) and the overtone of the folding modes O–C–O ($2\nu 2$), at 1270 and 1376 cm^{-1}, respectively [24]. Analysing the Raman Spectra of the CO_2 hydrates, a confirm about the similarity between gas-hydrates and ice water was given by the S_D index calculated from the spectra at – 60 °C of CO_2 hydrates; in fact, the results are comparable with the S_D index values of pure water (ice) in the same experimental condition (Fig. 10b). This confirms that, by studying the ice structure and the -OHs vibrations bands behaviour, it is possible to obtain useful information to predict the hydrates structures and the interaction between water molecules during the gas-hydrates formation.

3.4. CO_2-gas hydrates characterization by low temperature FE-SEM analysis

Fig. 12 shows low temperature- SEM images of CO_2 hydrates of pure water, formed with the equipment used for tests in Table 1, with and without sand showing different morphologies at different magnifications.

Specifically, at lower magnification, the surface morphologies of CO_2 hydrates (Fig. 12a) show cavity with dimensions of about tens micrometres typical of gas hydrates [28] while higher magnifications of the

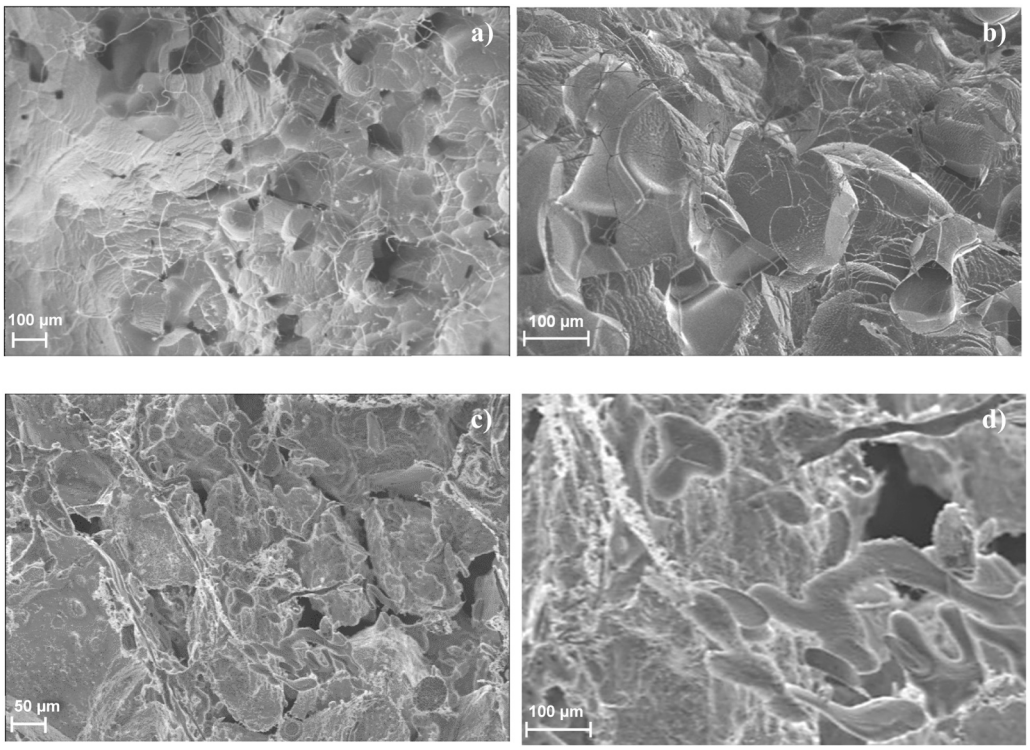

Fig. 12. SEM images of CO_2 gas hydrates in pure water (a,b) without and (c,d) with natural sand at different magnifications.

same sample (Fig. 12b) highlight the particular shapes of the cavities. When the CO_2 hydrates are formed in presence of natural sand, as reported in Fig. 12(c,d), a change in the morphology can be detected; in this case the structure is more dense and the morphology is more compact presenting similarity to that of natural gas hydrates where the sediments are present [8,29].

4. Conclusion

This study aims to identify knowledge gaps in CO_2 hydrate-based storage in marine environments. By analysing thermodynamic and kinetic parameters, this research provides insights into the effect of natural sand on the hydrate formation and dissociation. The novelty of this work lies in its integrated approach, combining macroscopic experimental results with microscopic analyses to establish a direct link between large-scale formation behaviour and microstructural characteristics.

Results of the hydrate formation and dissociation studies indicate a significant variation in hydrate formation dynamics in natural sediments when compared to pure water system, specifically:

- Gas uptake and formation density was considerably greater in natural sand as compared to the pure water system.
- The most influential operating parameter is temperature, in particular when temperature decrease gas uptake and formation density increase.
- CO_2 hydrate storage in natural sand represents a diffuse storage mechanism characterized by moderate storage densities when referred to the bulk porous medium. Compared to other geological storage approaches, this pathway benefits from solid-phase trapping and rapid formation timescales under favorable thermodynamic conditions, supporting its potential as a complementary storage option. The presence of sand was found to slow down hydrate dissociation under free-dissociation conditions.

RAMAN and SEM analyses explained the above mentioned trend as follows:

- CO_2 hydrates in natural sand present a denser and more compact morphology, similar to that of natural gas hydrates in sediment-rich environments.
- Sand organized the structure of water, with an increase of symmetric vibrations contribution at lower temperatures. This trend confirms that hydrate formation is higher at lower initial temperatures, when the structure is more organized.
- With ice water, the S_D index has the same behaviour (increasing with temperature and decreasing in presence of sediment); this result confirms the higher water conversion efficiency and density formation in presence of sand sediment.
- CO_2 hydrates share structural similarities with ice, particularly in the behavior of -OH vibrational bands. This insight helps predict hydrate structure and understand water-sediment interactions during formation.

Even though these findings can support the development of optimized hydrate-based CO_2 storage strategies in marine environments, further research is needed to better understand sediment-water interactions and the influence of factors like salinity on storage capacity and stability, so that a more complete comparison with other storage technologies can be carried out.

CRediT authorship contribution statement

Sowjanya Kandadai: Writing – original draft, Visualization, Resources, Investigation, Formal analysis, Data curation. **Umberta Tinivella:** Writing – review & editing, Supervision, Project administration, Funding acquisition, Formal analysis, Conceptualization. **Michela Giustiniani:** Writing – original draft, Validation, Resources, Investigation, Formal analysis, Data curation. **Lorenzo Remia:** Writing – original draft, Visualization, Resources, Investigation, Formal analysis, Data curation. **Beatrice Castellani:** Writing – review & editing, Validation, Supervision, Resources, Project administration, Methodology,

Investigation, Funding acquisition, Formal analysis, Data curation, Conceptualization. **Rita Giovannetti:** Writing – review & editing, Supervision, Formal analysis, Data curation. **Marco Zannotti:** Writing – review & editing, Validation, Supervision, Resources, Project administration, Investigation, Funding acquisition, Formal analysis, Data curation, Conceptualization.

Declaration of Competing Interest

The authors declare that they have no known competing financial interests or personal relationships that could have appeared to influence the work reported in this paper.

Acknowledgement

The aim of this work falls within the PRIN 2022 PNRR project entitled "Reliable long-term CO_2 storage as clathrate hydrates in seawater and marine sediments (CO_2-RESTO)", funded by the European Union – Next Generation EU and led by the University of Perugia, the University of Camerino, and the OGS Institute as research units.

Data availability

Data will be made available on request.

References

[1] IEA International Energy Agency (2022). CO2 Storage Resources and their Development. An IEA CCUS Handbook – Available online at: ⟨https://iea.blob.core.windows.net/assets/42d294af-ce07-44c7-9c96-166f855088e8/CO2storageresourcesandtheirdevelopment-AnIEACCUSHandbook.pdf⟩ (visited on June 17, 2025). Li Y. et al. (2024). Comprehensive characterizations of core sediments recovered from Shenhu W17 well in South China sea and its impact on methane hydrate kinetics. Gas Science and Engineering 131, 205482, https://doi.org/10.1016/j.jgsce.2024.205482.

[2] A. Bashir, M. Ali, S. Patil, M.S. Aljawad, M. Mahmoud, D. Al-Shehri, H. Hoteit, M. S. Kamal, Comprehensive review of CO_2 geological storage: exploring principles, mechanisms, and prospects, Earth-Sci. Rev. 249 (2024) 104672, https://doi.org/10.1016/j.earscirev.2023.104672.

[3] Malischek R. et al. (2021) The world has vast capacity to store CO2: Net zero means we'll need it. Available at: ⟨https://www.iea.org/commentaries/the-world-has-vast-capacity-to-store-co2-net-zero-means-we-ll-need-it⟩ (visited on June 17, 2025).

[4] E. Sloan, K.A.C. Dendy, Clathrate Hydrates of Natural Gases_Third Edition_Sloan.pdf, CRC Press, Taylor & Francis Group, Boca Raton, 2008.

[5] L. Wang, M. Dou, Y. Wang, Y. Xu, Y. Li, Y. Chen, L. Li, A review of the effect of porous media on gas hydrate formation, ACS Omega 7 (38) (2022) 33666–33679, https://doi.org/10.1021/acsomega.2c03048.

[6] P. Wang, Y. Teng, J. Zhu, W. Bao, S. Han, Y. Li, Y. Zhao, H. Xie, Review on the synergistic effect between metal–organic frameworks and gas hydrates for CH4 storage and CO2 separation applications, Renew. Sustain. Energy Rev. 167 (2022) 112807, https://doi.org/10.1016/J.RSER.2022.112807.

[7] X. Zhang, P. Li, Q. Yuan, J. Li, T. Shan, Q. Wu, Y. Wang, A comprehensive review of the influence of particle size and pore distribution on the kinetics of CO2 hydrate formation in porous media, in: Greenhouse Gases: Science and Technology, 13, John Wiley and Sons Inc, 2023, pp. 860–875, https://doi.org/10.1002/ghg.2239.

[8] B. Castellani, et al., Interdisciplinary results of an Italian research project on methane recovery and carbon dioxide storage in natural gas hydrate reservoirs, Green. Carbon 2 (2024) 351–365, https://doi.org/10.1016/j.greenca.2024.09.001.

[9] L. Ruffine, et al., Environmental challenges related to methane hydrate decomposition from climate change scenario and anthropic activities: State of the art, potential consequences and monitoring solutions, Earth-Sci. Rev. 246 (2023) 104578.

[10] M. Chaouachi, A. Falenty, K. Sell, F. Enzmann, M. Kersten, D. Haberthur, W. F. Kuhs, Microstructural evolution of gas hydrates in sedimentary matrices observed with synchrotron x-ray computed tomographic microscopy, Geochem. Geophys. Geosyst. 16 (6) (2015) 1711–1722, https://doi.org/10.1002/2015GC005811.

[11] K.U. Heeschen, J.M. Schicks, G. Oeltzschner, The promoting effect of natural sand on methane hydrate formation: Grain sizes and mineral composition, Fuel 181 (2016) 139–147, https://doi.org/10.1016/J.FUEL.2016.04.017.

[12] P.S.R. Prasad, Methane hydrate formation and dissociation in the presence of hollow silica, J. Chem. Eng. Data 60 (2) (2015) 304–310. ⟨https://pubs.acs.org/doi/abs/10.1021/je500597r⟩.

[13] T. Uchida, T. Ebinuma, S. Takeya, J. Nagao, H. Narita, Effects of pore sizes on dissociation temperatures and pressures of methane, carbon dioxide, and propane hydrates in porous media, J. Phys. Chem. B 106 (4) (2002) 820–826, https://doi.org/10.1021/jp012823w.

[14] Y. Li, et al., Tuning magnesium-induced CO_2 hydrate kinetics by hydrophilic and hydrophobic amino acids for effective hydrate-based CO_2 sequestration, Chem. Eng. J. 515 (2025) 163626, https://doi.org/10.1016/j.cej.2025.163626.

[15] E.M. Chuvilin, B.A. Bukhanov, Thermal conductivity variations of gas-saturated sediments during hydrate formation at different conditions. Part 2. Results, Earth'S. Cryosphere 18 (2) (2014) 49–55.

[16] L. Qi, M.D. Benitez, Z. Xia, J.C. Santamarina, Pore-scale phenomena in carbon geological storage (Saline aquifers—Mineralization—Depleted oil reservoirs), Front. Energy Res. 10 (2022), https://doi.org/10.3389/fenrg.2022.979573.

[17] F. Trippetta, A.M. Gambelli, G. Minelli, B. Castellani, F. Rossi, Sustainability of CO2 replacement processes in marine hydrate reservoirs: Factors causing changes on mechanical properties of Gas-Hydrate after CO2/CH4 exchange, Process Saf. Environ. Prot. 179 (2023) 628–639.

[18] J.M. Matter, M. Stute, S.Ó. Snæbjörnsdottir, E.H. Oelkers, S.R. Gislason, E. S. Aradóttir, B. Sigfusson, I. Gunnarsson, H. Sigurdardottir, E. Gunnlaugsson, G. Axelsson, H.A. Alfredsson, D. Wolff-Boenisch, K. Mesfin, D.F. Taya, de la Reguera, J. Hall, K. Dideriksen, W.S. Broecker, Rapid carbon mineralization for permanent disposal of anthropogenic carbon dioxide emissions, Science 352 (6291) (2016) 1312–1314, https://doi.org/10.1126/science.aad8132.

[19] M. Chaouachi, A. Falenty, K. Sell, F. Enzmann, M. Kersten, D. Haberthur, W. F. Kuhs, Microstructural evolution of gas hydrates in sedimentary matrices observed with synchrotron x-ray computed tomographic microscopy, Geochem. Geophys. Geosyst. 16 (6) (2015) 1711–1722, https://doi.org/10.1002/2015GC005811.

[20] A.N. Rehman, C.B. Bavoh, R. Pendyala, Z. Kassim, K.M. Sabil, N.A.B. Othman, B. Lal, Kinetic insight on CO_2 hydrate formation and dissociation in quartz sand in presence of brine, in: International Journal of Greenhouse Gas Control, 114, Elsevier Ltd, 2022, https://doi.org/10.1016/j.ijggc.2022.103582.

[21] J. Choma, J. Jagiello, M. Jaroniec, Assessing the contribution of micropores and mesopores from nitrogen adsorption on nanoporous carbons: Application to pore size analysis, Carbon 183 (2021) 150–157.

[22] Q. Sun, The Raman OH stretching bands of liquid water, Vib. Spectrosc. 51 (2009) 213–217.

[23] Q. Sun, H. Zheng, Raman OH stretching vibration of ice I_h, Prog. Nat. Sci. 19 (2009) 1651–1654, https://doi.org/10.1016/j.pnsc.2009.06.010.

[24] R. Giovannetti, et al., May sediments affect the inhibiting properties of NaCl on CH4 and CO2 hydrates formation? An experimental report, J. Mol. Liq. 359 (2022) 119300.

[25] R. Mancinelli, et al., Perturbation of water structure due to monovalent ions in solution, Phys. Chem. Chem. Phys. 9 (2007) 2959–2967, 2007.

[26] D.A. Schmidt, K. Miki, Structural Correlations in Liquid Water: A New Interpretation of IR Spectroscopy, J. Phys. Chem. A 111 (40) (2007) 10119–10122.

[27] I. Đuričković, et al., Experimental Study of NaCl Aqueous Solutions by Raman Spectroscopy: Towards a New Optical Sensor, Appl. Spectrosc. 64 (8) (2010) 853–857.

[28] R. Giovannetti, et al., Thermodynamic assessment and microscale Raman spectroscopy of binary CO2/CH4 hydrates produced during replacement applications in natural reservoirs, J. Mol. Liq. 368 (2022) 120739.

[29] J. Sun, C. Li, X. Hao, et al., Study of the Surface Morphology of Gas Hydrate, J. Ocean Univ. China 19 (2020) 331–338, https://doi.org/10.1007/s11802-020-4039-7.

[30] Y. Li, et al., Comprehensive characterizations of core sediments recovered from Shenhu W17 well in South China sea and its impact on methane hydrate kinetics, Gas Sci. Eng. 131 (2024) 205482, https://doi.org/10.1016/j.jgsce.2024.205482. https://doi.org/10.1016/j.jgsce.2024.205482.

[31] G.J. Speight, Chapter 4 - Hydrocarbons from natural gas and natural gas hydrates, in Handbook of Industrial Hydrocarbon Processes (Second Edition), Gulf Professional Publishing-Elsevier, 2020, pp. 143 - 192. https://doi.org/10.1016/B978-0-12-809923-0.00004-7.